

# Computational studies of pairwise repulsions in the carbon monoxide/platinum(111) surface system

A J Gordon-Wright

Department of Physics, University of Bath, Bath BA2 7AY, United Kingdom

E-mail: ajgw20@bath.ac.uk

**Abstract.** Monte Carlo simulations, using the conserved-order parameter Ising model with Kawasaki dynamics, are used to simulate the dynamics of CO molecules adsorbed on a Pt(111) surface. The intermediate scattering function  $I(\mathbf{k},t)$  is calculated along the  $\langle 11\bar{2} \rangle$  crystal azimuth for CO coverages  $\theta$  ranging from 0.065 - 0.4 monolayers, with a pairwise lateral CO repulsion  $E_{\text{rep}}$  ranging from 0 – 100meV. The dependence of the inverse lifetime of this function on  $\mathbf{k}$  for different coverages and repulsions is used to show that there is a very small upper limit on  $E_{\text{rep}}$  to produce uncorrelated surface motion of CO adatoms. This limit is on the order of 50meV for low coverages, but only 10meV for larger coverages. Comparing this to previously published results suggests that the magnitude of the repulsion often proposed as roughly 40meV may be too large. In addition, a method for directly calculating the interaction energy from density functional theory calculations is proposed.

## 1. Introduction

The carbon monoxide/platinum(111) [CO/Pt(111)] system is extremely widely studied. Platinum is an important industrial catalyst, and the study of this particular system has important applications, for example in Fischer-Tropsch synthesis of liquid fuels from CO and H<sub>2</sub> [1], and in the mechanism of catalytic conversion in car exhausts. The CO/Pt(111) system consists of CO adatoms bound to a Pt(111) surface. Pt forms a face-centred cubic (f.c.c.) lattice when in bulk form [2]. A cell of this lattice is shown in figure 1(a). The (111) plane indices give the grey plane shown on the figure. Cleaving the bulk material to expose this plane gives a surface like 1(b). This is a hexagonal lattice (so called because it has six-fold rotational symmetry; the repeating unit cell is actually a parallelogram as shown). The bulk lattice parameter  $a_{\text{Pt}}$  shown determines the overall scale of the system, however units are usually chosen, and will generally be here, so that  $a_{\text{Pt}}/\sqrt{2}=1$ . When CO binds to the Pt(111) surface, it can do so at one of four potential binding sites, marked 1-4 on figure 1(b). The f.c.c. and h.c.p. hollow are different due to the underlying bulk layers below the surface. These four different sites can have slightly different binding energies, a fact which has proven hard to simulate accurately in the past [3].

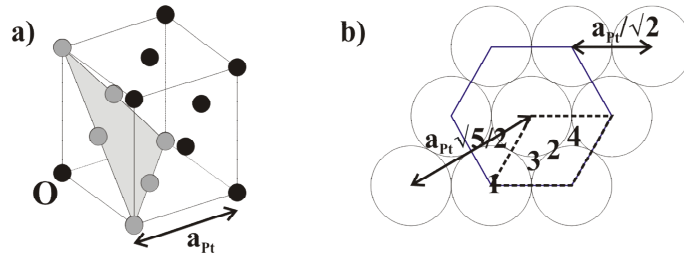


**Figure 1.** a) The bulk fcc lattice cell with origin O, showing the (111) plane (grey) and the atoms on it, and the bulk lattice constant  $a_{\text{Pt}}$ . b) The (111) surface plane, showing the primitive unit cell (dashed line), the hexagonal cell, and the four potential binding sites. 1: top site, 2: bridge site, 3: f.c.c. hollow site, 4: h.c.p. hollow site.

Previous studies of this system show a reduction in the CO heat of adsorption as the surface coverage  $\theta$  of CO increases. ( $\theta$  is expressed as the fraction of adatoms relative to the number

of surface atoms.) These studies include those using single crystal absorption calorimetry [4-5], thermally programmed desorption and work function measurements [6]. Other techniques also show coverage-dependent results: for example a shift in the CO vibrational frequency in infrared reflection-absorption spectroscopy [7-8], and changes in diffraction patterns in low-energy electron diffraction [6, 9]. Results also suggest the existence of certain preferred ordered structures at different coverages, for example the  $(\sqrt{3}\times\sqrt{3})R30^\circ$  structure at  $\theta=0.33$  [6], and the  $c(4\times2)$  structure at  $\theta=0.5$ . These structures are shown in figure 2(a) and (b). These structures have the maximum possible inter-adatom separation at these coverages.

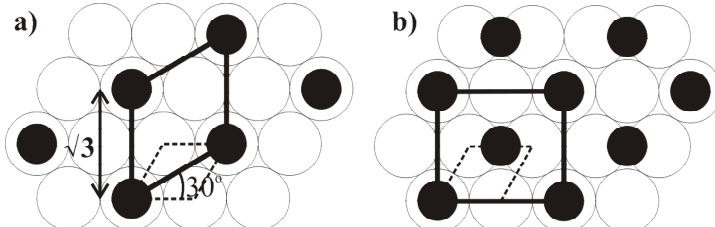


**Figure 2.** a)  $(\sqrt{3}\times\sqrt{3})R30^\circ$  adatom ordering. b)  $c(4\times2)$  adatom ordering. Both show surface atoms (empty circles), adatoms (filled circles), the respective unit cells (solid lines), and the primitive surface unit cell (dotted line) for comparison.

It is a frequent assumption of the analyses of these studies, eg. [4, 9-10], that these results are explained by a pairwise lateral repulsion between CO adatoms. As coverage increases, each CO adatom is forced closer to other CO adatoms, increasing the repulsion it feels therefore reducing the heat of adsorption. Simulations of this system also frequently use this assumption when designing the dynamics [11-14]. However, a recent study by Alexandrowicz *et al.* [15] shows intriguing results that cast this assumption into doubt. They suggest that CO interactions could not be of the separable pairwise form (i.e. acting between pairs of CO adatoms, depending only on their separation). Rather, they must take a more complicated many-body form. These results are made possible by the development of a new experimental technique called helium spin-echo spectroscopy ( $^3\text{He-SE}$ ) [16-17]. The primary goal of this study is to shed some light on this disparity. This is accomplished through Monte Carlo simulations to attempt to find parameters that will reproduce these results. In addition, a suggestion is given, and partially executed, for how *ab initio* density functional theory calculations may reveal the strength of any interactions.

### 1.1. The intermediate scattering function (ISF)

The quantity measured by  $^3\text{He-SE}$  experiments is proportional to the intermediate scattering function,  $I(\mathbf{k}, t)$ . This measures the scattering cross-section of the surface for a given reciprocal space vector  $\mathbf{k}$ , also called the momentum transfer, over time  $t$ . It is given by:

$$I(\mathbf{k}, t) = \int_{\mathbf{r}} d\mathbf{r}^2 \exp(i\mathbf{k} \cdot \mathbf{r}) G(\mathbf{r}, t), \quad (1)$$

where  $G(\mathbf{r}, t)$  is the Van Hove pair correlation function [18], and the integral is over all vectors  $\mathbf{r}$  within the surface plane. It can be shown that this quantity decays exponentially with time for a given  $\mathbf{k}$  [11]. However, the decay rates for different  $\mathbf{k}$  will also potentially be different. Pairwise repulsive interactions will tend to result in certain transient ordered surface structures, and hence certain interatomic separations  $\mathbf{r}_0$ , having increased lifetimes. This in turn leads to a shorter inverse lifetime,  $\alpha(\mathbf{k})$ , for  $I(\mathbf{k}_0, t)$ , where  $\mathbf{k}_0 \cdot \mathbf{r}_0 = 2\pi$ . This shift will be highly coverage dependent: at lower coverages, each CO is on average not close enough to other adatoms to feel much repulsion. As the coverage is increased, the effect is increased, but only for certain values of  $\mathbf{k}$ .  $\alpha(\mathbf{k})$  therefore has a changing functional form for increasing coverage when pairwise lateral repulsions are included. However, in [15], a constant functional form fits the data for all coverages with a simple scaling factor, which ultimately suggests a lack of pairwise repulsions.

## 2. Monte Carlo study

The present study primarily consists of developing a Monte Carlo simulation of the CO/Pt(111) system to generate  $I(\mathbf{k}, t)$  for varying coverages. Monte Carlo techniques are a class of stochastic simulation methods [19]. They are used in the study of many different systems, for example [20-22]. Their probabilistic approach is an efficient way to reduce the computational complexity of a calculation involving a many-body problem.

Monte Carlo methods rely on randomly selected moves being accepted with a certain probability. Generally speaking, the probability that a particle will have enough energy for the move is used, picked from the Boltzmann probability distribution. The move is then accepted or rejected with this probability, and the next move selected. In conventional Monte Carlo simulations, each time step (called a sweep) includes a number of these moves equal to the total number of objects in the system (although the object used in each move is picked randomly), so that on average each object moves or attempts to move each time step [23]. This gives realistic dynamics, and is much more efficient than simulating fully the dynamical system involved. Advanced methods use variations on what is called continuous time Monte Carlo, where each selected move is accepted, and a time variable is updated each move with the length of time required for the move to have happened on average, for example [11, 24].

### 2.1. Computational details

In the present study, a conserved-order-parameter Ising model [23] with Kawasaki dynamics [25] is used. Whilst more efficient models exist, this model is still expected to give reasonable results in a reasonable period of time. The CO adatoms are represented by a lattice gas model, with each CO occupying one vertex of a two-dimensional lattice which represents the available binding sites on the surface. The total lattice size is set in terms of the number of surface unit cell vectors in each direction. In this case, only the top sites are included in the calculation. This is a major approximation, but one which may still provide valid results at low coverages. For low coverages, CO prefers binding to top sites [3]. It is only for coverages increasing towards  $\theta=0.5$  that CO binds in significant numbers to other sites. Coverages above 0.4 are therefore not investigated in this study. Each lattice site has a value of 1 or 0 showing its occupation. The CO atoms diffuse around the lattice, with the underlying surface having no effect except to set the lattice shape. If other sites were included, the differences in binding energies between sites would also affect the motion of the CO, but as all sites are the same in this model this is not the case.

Two factors affect the motion of the CO. The first is that each lattice site can only have one CO, so if the randomly selected move involves a CO moving to an already occupied site, the move is rejected. The second is a pairwise repulsion, acting only on nearest-neighbour COs, which can be varied. This means that moves where a CO moves to a site with more nearest-neighbours than its current site are energetically unfavourable, and have a small probability of acceptance. By contrast, moves where the number of nearest-neighbours is reduced have an acceptance probability of 1. The algorithm of each sweep is therefore as follows:

1. Select a random adatom to move.
2. Select a random nearest-neighbour to move it to. If the nearest-neighbour is already occupied, reject and go to 1.
3. If not, accept the move with a probability,  $P$ , determined by the change in the number of nearest-neighbours,  $\Delta_{nn}$ :

$$P(\Delta_{nn}) = \begin{cases} 1 & \Delta_{nn} \leq 0 \\ \exp(-\beta \Delta_{nn} E_{rep}) & \Delta_{nn} > 0 \end{cases}, \quad (2)$$

where  $\beta = 1/k_B T$ , with  $k_B$  Boltzmann's constant and  $T$  the simulation temperature, and  $E_{rep}$  is the specified pairwise repulsive interaction. The simulation temperature used here is always 340K, as this is the temperature used in [15].

4. Repeat this process for a number of moves equal to the number of CO adatoms.

To calculate  $I(\mathbf{k}, t)$  for this simulation, (1) must be put in a different form. With this discrete lattice geometry, the integral over all space can be changed to a sum over the possible lattice vectors. Using the fact that the only possible densities are 1 or 0, thus reducing the sum to a sum over only occupied sites, a slight rearrangement then gives:

$$I(\mathbf{k}, t) = \frac{1}{N} \sum_i \exp[i\mathbf{k} \cdot \mathbf{r}_i(t)] \sum_j \exp[-i\mathbf{k} \cdot \mathbf{r}_j(0)] \}, \quad (3)$$

where  $\mathbf{r}_n(t)$  is the positional vector of atom  $n$  at time  $t$ , and  $N$  is the number of adatoms on the lattice. This is a very useful result. The two sums are exactly equivalent to the complex conjugate of the Fourier transform of the particle positions at time  $t$  and the Fourier transform of the particle positions at time 0 respectively. To calculate the ISF for a given time, all that is required is to Fourier transform the lattice at time 0, then again at time  $t$  (taking the complex conjugate here), and multiply the two together at any  $\mathbf{k}$  points required. This can be a very fast process using a Fast Fourier transform routine. In this case, the FFTW3 library [26] was used for the transformations. The overall algorithm for the program is then:

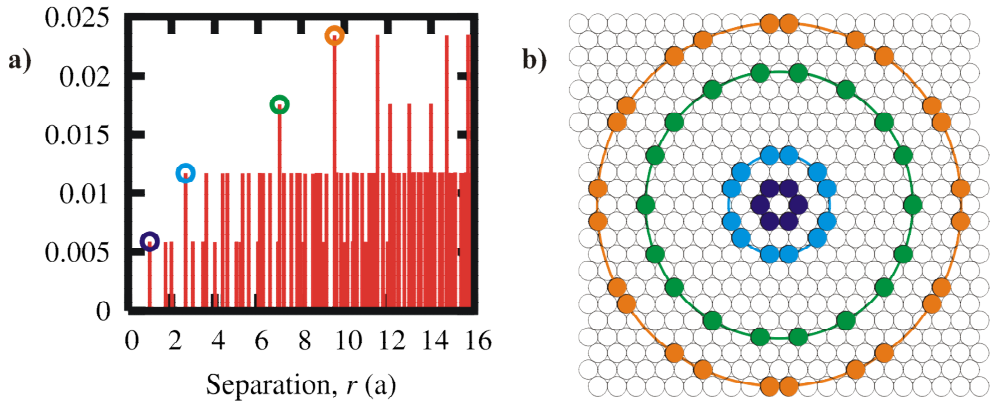
1. Place required number of adatoms at random sites on the lattice.
2. Allow simulation to run for a certain number of sweeps to come to the correct temperature. This is because random adatom positions are equivalent to  $T=\infty$ , when motion is completely random, hence this starting position is not strictly accurate for the temperature being simulated.
3. Fourier transform the adatom positions and store the result as  $t=0$ .
4. For a selection of other time steps, store the Fourier transform.
5. Multiply the complex conjugate of the higher time step transforms with the  $t=0$  transform for a selection of points in  $\mathbf{k}$ -space, to give  $I(\mathbf{k}, t)$ . In this case, points along the  $<11\bar{2}>$  crystal azimuth were chosen to better compare with [15].
6. Set the current transform to be the  $t=0$  transform and repeat from 4. Store the mean values of  $I(\mathbf{k}, t)$ , as well as the mean squared values for calculating the variance.
7. After a set number of repeats, output the mean and variance.

*2.1. Static pair correlation.* Whilst developing the simulation, it is important to test that it is behaving as expected. At an early stage it is possible to implement a calculation of the static pair correlation function,  $G(r)$ , given by:

$$G(r) = \frac{\sum_{i,j \text{ with } r=|\mathbf{r}_i - \mathbf{r}_j|} <\rho(\mathbf{r}_i)\rho(\mathbf{r}_j)>}{\sum_{i,j} <\rho(\mathbf{r}_i)\rho(\mathbf{r}_j)>} [18], \quad (4)$$

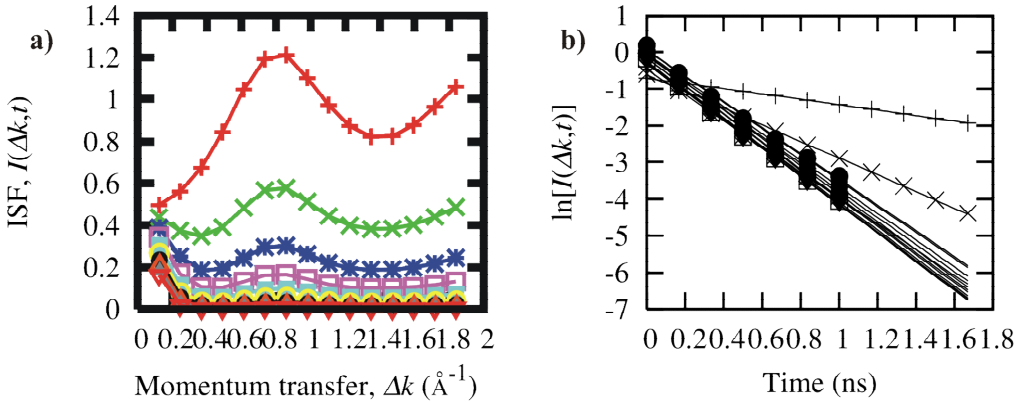
where  $\rho(\mathbf{r})$  is the density at position  $\mathbf{r}$ , and the sum is over all lattice sites. This represents the probability of finding an atom at position  $r$  given that there is one at  $r=0$ .

Figure 3(a) shows a typical pair correlation function, calculated on a 32x32 lattice, with no pairwise repulsion, at a coverage of  $\theta=0.1$ . There is also a correlation of unity at  $r=0$  by definition. Only certain separations are possible, due to the discrete nature of the lattice. The probability of finding an atom at a certain distance is proportional to the number of atoms that can occupy this “shell”, as would be expected. For example, the four peaks shown on 2(a) are the first shells with 6, 12, 18 and 24 nearest-neighbours respectively, as illustrated in 2(b). These results then are entirely consistent with expectations.



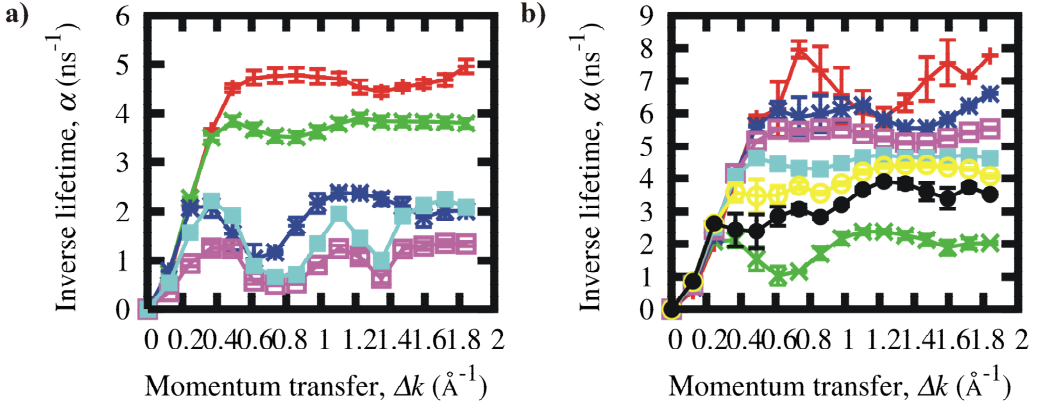
**Figure 3.** a) Pair correlation function  $G(r)$  with simulation dimension  $L=32$ ,  $E_{\text{rep}}=0$  and  $\theta=0.1$ , with the peaks at  $r=1$  (purple), 2.65 (blue), 7 (green) and 9.54 (orange) marked. b) Lattice showing the atoms detected by these peaks (same colours).

**2.2. Method of analysis.** A sample of the initial program output is shown in Figure 4(a).  $I$  is now given as a function of  $\Delta k$  rather than  $k$ , where  $\Delta k=|k|$  along the  $\langle 11\bar{2} \rangle$  crystal azimuth, as the results are all along the same unit vector.  $\Delta k$  was recorded up to the first Brillouin zone (BZ) boundary, as the behaviour of the system over all  $k$ -space can be described by its properties within the first BZ, analogous to how the behaviour in real space is determined by properties within the primitive unit cell. The decay of  $I(\Delta k, t)$  over even such a short time as 10 Monte Carlo steps is marked.  $I(0, t)$  and  $I(\Delta k, 0)$  are not shown, as they are by definition constant, which can easily be shown from (3). The part shown here is the real part of the ISF, as the imaginary part averages out to zero over time. In addition, error bars are not shown as the calculated standard deviations in the results are too small to show.



**Figure 4.** a) ISF as a function of momentum transfer for a run over ten successive Monte Carlo steps, with  $E_{\text{rep}}=100\text{meV}$  and  $\theta=0.1$ . The first step is the orange line with crosses, with each successive step being uniformly smaller than the last. b) Exponential decays in ISF at each point in  $k$ -space, from (a). Successive  $k$ -point series of increasing  $k$  value are shown by +, x, then various largely obscured symbols due to the similar lifetimes of different series.

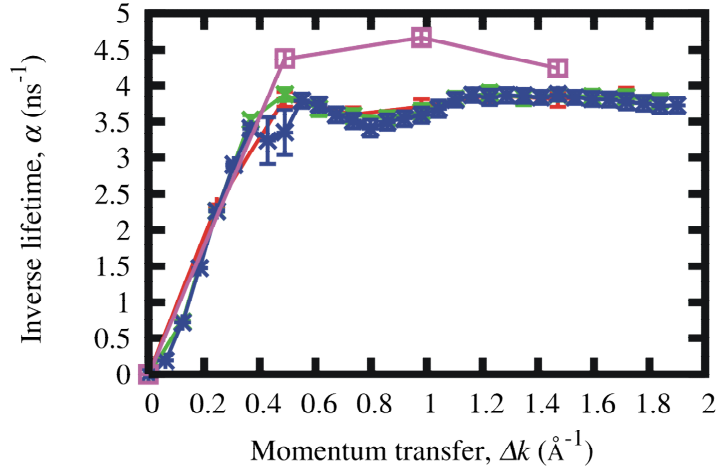
To analyse results such as this, the inverse lifetime  $\alpha(\Delta k)$  of the ISF is calculated for each  $\Delta k$  value by fitting an exponential decay to the results such as Figure 4(a), using a logarithmic fit. Figure 4(b) is a log plot to show these fits. The plotted lines represent fitted functions for each data set of the form  $\ln(I)=-\alpha t+c$ , with the negative gradient being equal to  $\alpha(\Delta k)$ . Values that have decayed by  $e^4$  are removed from the end of the dataset for each  $\Delta k$ , as when the ISF has decayed by a large amount there is a lot of noise in the data. Finally,  $\alpha$  is plotted against  $\Delta k$ , as in figure 5(a). The errors on  $\alpha(\Delta k)$  are calculated simply from the errors in the least squares regression of  $\ln[I(\Delta k, t)]$ .



**Figure 5.** Inverse lifetimes against  $\Delta k$ , for: a) coverages of 0.065 (orange), 0.1 (green), 0.2 (purple), 0.3 (pink) and 0.4 (blue) with  $E_{\text{rep}}=100 \text{ meV}$ ; and b)  $E_{\text{rep}}=0$  (orange), 10 (purple), 20 (pink), 30 (blue), 40 (yellow), 50 (black) and 100 (green) meV, with  $\theta=0.2$ .

The time scale in 4(b) is calculated as follows. Firstly, a run is made at low coverage ( $\theta=0.065$ ) with no repulsion, and analysed to give results for  $\alpha(\Delta k)$ . This is then compared to the low coverage  $\alpha(\Delta k)$  measurement in [15]. By assuming the same functional form for both sets, a simple scaling factor is found that maps the results from this study roughly on to the previous results. This factor is equal to the timescale per Monte Carlo step,  $\tau_0$ , due to the relationship between  $\alpha(\Delta k)$  and the timescale. This gives  $\tau_0 = 0.17 \pm 0.03 \text{ ns}$ . This can then be used to compare the computational results roughly to real results. Note that the error contribution from this uncertainty in the timescale is not shown in figure 5, as the important task is to compare results from simulations with different parameters. Comparing the results qualitatively with previous work is useful; however quantitative comparisons are not strictly necessary. Hence, this time scale estimate is only used to put a rough scale on the results.

**2.3. Finite size scaling.** An important parameter determining the accuracy of Monte Carlo simulations (and indeed of many other computational methods) is the lattice dimension  $L \times L$  of the simulation. As the system uses periodic boundary conditions, with the lattice repeated infinitely in space, too small simulations will result in unrealistic finite size effects, as an atom interacts with mirrors of itself in neighbouring cells.



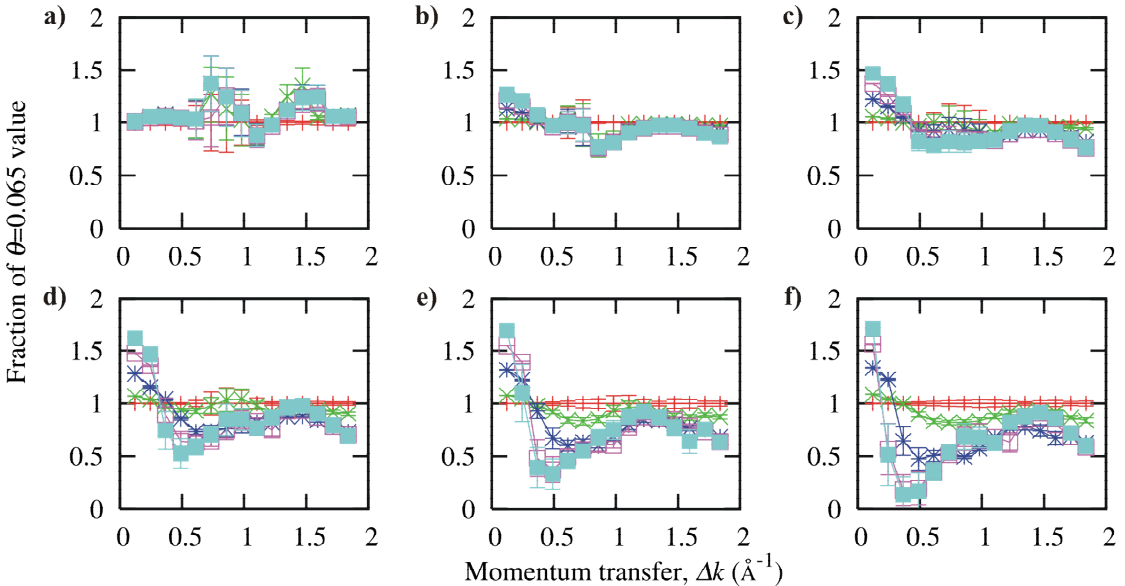
**Figure 6.** Finite size scaling effects. The ISF is shown over the first BZ with  $L=8$  (pink), 16 (orange), 32 (green) and 64 (purple).

Figure 6 shows this effect. Fortunately, it can be seen that the results quickly converge with increasing cell size. Up to this point, an arbitrary size  $L=32$  has been used. There is not a significant difference between this and the result for  $L=64$ , apart from around  $\Delta k = 0.4 \text{ \AA}^{-1}$ , where the statistical errors are large anyway. There is however a large difference in the

length of the simulation, which scales with  $O(L^2)$ . As  $L$  can only be a power of 2 (due to certain speed increases this allows in the calculation),  $L=32$  is used for the rest of this study.

**2.4. Effects of coverage and repulsions.** Figure 5(a) shows the effect of increasing coverage on  $\alpha(\Delta k)$  for a fixed  $E_{rep}$  of 100meV. In general, increasing coverage reduces the inverse lifetime, showing therefore an increased lifetime of surface structures. This would be due to both the increase in the number of moves rejected as adatoms try to move to occupied states, and the reduced probability of many moves as they would increase the number of nearest-neighbours. It should be noted that the effect appears to be of a different magnitude for different coverages (whilst the low coverage  $\theta=0.065$  measurement is roughly flat after  $\Delta k = 0.4 \text{ \AA}^{-1}$ , for higher coverages the pattern has significant modulations). This suggests as previously mentioned that there are certain preferred real-space separations  $r$  for higher coverages, corresponding to ordered surface structures, which lead to reductions in  $\alpha(\Delta k)$  where  $\Delta k \cdot r = 2\pi$ . It should also be noted that the structure with the longest lifetimes occurs at  $\theta=0.3$ . This probably corresponds roughly to the  $(\sqrt{3}\times\sqrt{3})R30^\circ$  structure shown in figure 2(a), which has  $\theta=0.33$ , as this is modelled well by the present simulation. The structure involves only top site adsorption, and includes full nearest-neighbour exclusion (each CO adatom is surrounded by empty sites). Figure 5(b) shows the effect of increasing repulsions on  $\alpha(\Delta k)$  for  $\theta=0.200$ . The significant reduction in  $\alpha(\Delta k)$  for increasing repulsions can clearly be seen. Further results (not shown) for this coverage show that repulsions greater than or equal to 200meV give essentially identical results to each other, suggesting an upper limit on repulsive effects.

**2.5. Cut-off for uncorrelated motion.** Figure 7 shows a combined picture of the effects of coverage and repulsion, with the changes in  $\alpha(\Delta k)$  caused by increasing coverage shown for various interaction strengths. The changes are compared by expressing  $\alpha(\Delta k)$  for each coverage as a fraction of the  $\theta=0.065$  measurement, so that a value of less than one shows a reduced inverse lifetime caused by the increased coverage. Uncorrelated surface motions lead to a uniform reduction in  $\alpha(\Delta k)$  for increasing coverage, so the fraction should be constant across each data set with uncorrelated motion.



**Figure 7.** Coverage and interaction dependent change in inverse lifetimes shown by expressing results as a fraction of the low coverage measurement for interaction strengths of: a) 0 meV, b) 10meV, c) 20meV, d) 30meV, e) 40meV and f) 50meV. The different coverages are: 0.065 (orange), 0.1 (green), 0.2 (purple), 0.3 (pink), 0.4 (blue).

For no repulsion, the results are essentially the same for increasing coverage, with the fractions all clustered around 1 (with points further away from 1 having large error bars).

However, even for repulsions of 10meV, some small correlation effects show, and by 30meV only the  $\theta=0.1$  series could be said to show no correlated motion effects. By 40meV, all coverages show a non-uniform reduction in  $\alpha(\Delta k)$ .

### 3. Density functional theory calculations

A second way to approach this problem computationally is through the employment of density functional theory (DFT). DFT is an approach to solving the analytically intractable many-body Schrödinger equation problem, using only a small number of approximations (in the simplest theoretical case, only one approximation is made). DFT calculations are also called *ab initio* or first-principles calculations [27], as they start from the equation that exactly describes the problem.

DFT is based on two major papers, the first by Hohenberg and Kohn [28], and the second by Kohn and Sham [29]. These papers show that the problem of many interacting electrons can be expressed as the problem of the same number of non-interacting electrons, interacting with an effective potential which consists of contributions from any external potential and from other electrons. Through a cycle which takes a starting electron density  $n(\mathbf{r})$ , calculates the effective potential from this, then the electron wavefunctions, then a new electron density, the total energy can be converged. In principle, this should give an exact solution. However, this process is complicated by the fact that the effective potential includes contributions from the so-called exchange-correlation energy, which describes contributions from the effects of swapping two electrons (exchange), and from electron correlations [19]. This also depends on the density, but is not analytically known. Much work on DFT involves designing new exchange-correlation functionals, from the original local density approximation (LDA) [29], to the generalised gradient approximation (GGA), which takes account of the gradient of electron density at each point as well as the magnitude [19], and beyond.

The use of DFT for studying the CO/Pt(111) system has previously been called in to question [3]. In particular, it was suggested that it does not show the correct energy preference for certain binding sites. However, later results suggest that this might not be the case, and that incorrect predictions are more likely to be due to random experimental errors than systematic problems [30-31]. By DFT using it to calculate the total energies of different configurations of CO molecules on the surface, a link can be looked for between inter-adatom separation and total energy. If the energy increases as the adatoms get closer together, then this strongly indicates a repulsive interaction. Initial calculations have been made to determine a method for this, but the final calculations have not yet been carried out.

#### 3.1. Computational details

DFT calculations are here carried out on a supercomputing cluster. The PW-SCF [32] DFT package, which is freely available software, is used. The PW here stands for plane-wave, in that the electron wavefunctions are expanded as plane waves, and SCF stands for self-consistent field, referring to the self-consistency conditions. Various pseudopotentials (PPs) were used. These are potentials which represent the core electrons in an atom with an effective potential, thus requiring the full DFT calculation to be carried out only on the valence electrons.

#### 3.2. CO test runs

The first calculations carried out are used to determine the suitability and accuracy of the software for calculations involving CO. These are carried out on isolated CO molecules in free space. (An important point to note is that DFT calculations always use periodic boundary conditions, so in fact these are calculations on an array of CO molecules separated by suitably large distances.) The C atom is positioned at one vertex of the unit cell, with the O atom positioned initially at a separation of  $r$  away. Two main types of DFT calculation can be run on this system: single SCF cycle calculations, where atoms are kept fixed and the energy is minimised, and relaxation calculations. These utilise the fact that at the end of each SCF

cycle the residual force on all atoms is known. By slightly moving the atoms in the direction of this force and running another SCF cycle, and repeating this as much as necessary, the geometry which gives the lowest total energy can be found, giving things like equilibrium separations  $r_0$ , as well as a better total energy value.

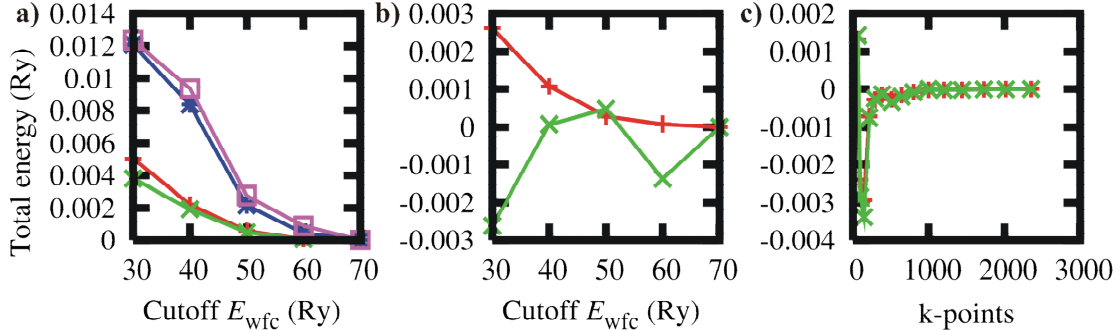


**Figure 8.** Total energy convergence with respect to  $E_{wfc}$  and k-points, for various GGA/LDA and PP combinations. a) Relaxation calculation on free space CO, energy relative to that at  $E_{wfc}=70\text{Ry}$ ; b) single SCF cycle calculation on bulk Pt, energy relative to that at  $E_{wfc}=70\text{Ry}$ ; c) k-point convergence for bulk Pt, energy relative to that at 2352 k-points. Combinations used: PZ-RRKJUS (orange), PBE-RRKJUS (green), PBE-VAN (purple), and PW91-VAN (pink).

This geometry is then used to investigate some parameters of the calculation: the wavefunction plane-wave energy cut-off,  $E_{wfc}$ , the electron density plane-wave energy cut-off,  $E_{rho}$ , the LDA or GGA used, and the type of PP.  $E_{wfc}$  and  $E_{rho}$  are used in the plane-wave expansions of the wavefunctions and electron densities respectively to truncate the number of waves used to a finite amount, to allow calculation. These are important parameters of the simulation: increasing them leads to a more accurate expansion, and therefore more accurate results, but significantly slows down the calculation. Figure 8(a) shows how the total energy of the calculation converges as  $E_{wfc}$  is increased. The lines correspond to the LDA due to Perdew-Zunger (PZ) [33] with ultrasoft pseudopotentials (USPs) [PZ-RRKJUS], and the GGA due to Perdew-Burke-Ernzerhof (PBE) [34] with USPs [PBE-RRKJUS], PBE with Vanderbilt PPs (PBE-VAN), and Perdew-Wang 91 (PW91) [35] with Vanderbilt PPs (PW91-VAN). All of these combinations also give different total energies and equilibrium separations, with the LDA in particular thought to overestimate total energies [3], as found in the present study. In this case, PBE-GGA with USPs showed the fastest convergence with respect to  $E_{wfc}$ , so this combination is generally used hereafter. The dependence on  $E_{rho}$  can also be investigated. Results (not displayed here) show that this cut-off needs to be roughly ten times higher than  $E_{wfc}$  for the same level of convergence. To get a balance between speed and accuracy,  $E_{wfc}=40\text{Ry}$  is generally used hereafter ( $1\text{Ry} = 13.6\text{eV}$ , the ground state energy of the hydrogen atom).  $E_{rho}$  is then set as  $400\text{Ry}$ .

A relaxation calculation gave the bond length of CO as  $1.130 \pm 0.006\text{\AA}$ , which is the same as the experimental value [36]. The vibrational frequency of the bond could also be calculated, by modelling the bond as a harmonic oscillator for small displacements around the equilibrium bond length [37].  $r$  can be fixed at various values, and the total energy calculated. Then by fitting a parabola to these results, the force constant of the bond can be found, which gives the frequency and hence the wavenumber  $\nu$ . The result here was  $\nu=2163 \pm 10\text{cm}^{-1}$ , again in good agreement with the experimental value of  $2143\text{cm}^{-1}$  [7].

### 3.3. Pt test runs

Cut-off convergence for platinum must be tested as well. Figure 8(b) shows this convergence for platinum arranged in its f.c.c. unit cell [as shown in figure 1(a)]. The result is again reasonably well converged for  $E_{wfc}=40\text{Ry}$ , so this value is used later. One other factor that must be investigated for this more complicated geometry is the convergence with respect to the number of k-points used. The k-points are the points in reciprocal space at which energies

are sampled. More points gives more accurate results, but again at the expense of speed. Figure 8(c) shows this convergence rate. The smallest cubic arrangement that is converged here is at 1000 k-points. Using this value, the equilibrium bulk lattice parameter of platinum is found to be  $a_{\text{Pt}}=4.00\text{\AA}$  using a relaxation calculation. This agrees well with the accepted value. The bulk modulus of platinum is calculated as  $K=238\text{GPa}$ , again in good agreement with previous data.

### 3.4. The full surface system

The full system is set up through the use of a “supercell”. In the x-y plane, a certain square number of primitive unit cells is taken (1 to start with). This prism is then extended through 5 Pt(111) layers, then a further 7 layers equivalent of free space. This gives, with periodic boundary conditions, an infinite number of 5 layer thick slabs extending to infinity in the x and y directions, separated by 7 layers of vacuum in the z direction. CO molecules can then be placed on different binding sites on the exposed surface layer. Further k-point convergence tests show that a  $24\times 24\times 1$  grid is sufficient to accurately represent the system with a  $1\times 1$  surface unit cell. The system is first set up with dimensions calculated from the  $a_{\text{Pt}}$  found earlier. A relaxation calculation is then run with the top two Pt layers allowed to relax (the bottom three are treated as bulk). The top layer relaxes outwards by  $0.002\text{\AA}$ , whilst the layer below relaxes into the bulk by  $0.015\text{\AA}$ . These new positions are then used as the initial positions when adding CO.

### 3.5. Preliminary results

Binding energies for different sites, coverages and separations can now be investigated. Preliminary investigations show that, for a  $1\times 1$  unit cell with a coverage of  $\theta=1$ , the top site is the preferred site, by 38meV over the f.c.c. hollow, 90meV over the h.c.p. hollow, and 267meV over the bridge site. These results are consistent with predicted low coverage results [3], but not with the fact that bridge sites appear to be more favoured as coverage increases [6]. Further calculations are now required for larger cells, with therefore lower possible coverages, and for different adatom geometries.

## 4. Discussion

The  $\alpha(\Delta k)$  results, for different coverages and repulsion strengths, clearly show the effects of correlated motion. The effects are particularly great for the  $\Delta k$  points corresponding to the real-space separations of the second and third nearest-neighbours. When pairwise repulsions are present, for all except low coverages these separations become on average more common and longer lasting (as atoms get forced out of the first nearest-neighbour shell into these ones). This results in these separations being longer-lasting, hence having short inverse lifetimes. Going back to figure 7, a rough figure for the strength of interaction at each coverage that will not result in correlated motion can be obtained. These are found to be:  $E_{\text{rep}} < 50\text{meV}$  for  $q=0.065$ ,  $E_{\text{rep}} < 30\text{meV}$  for 0.1,  $E_{\text{rep}} < 20\text{meV}$  for 0.2, and  $E_{\text{rep}} < 10\text{meV}$  for 0.3 and 0.4.

These results would seem to back up the primary conclusion found in [15]: namely that a separable pairwise repulsion cannot be assumed. They show that uncorrelated motions only occur for extremely small interactions within this model. These interactions are generally smaller than the proposed interaction strengths in various papers, for example [9-11]. However, the fact that some small interactions do not result in correlated motion (probably primarily due to thermal fluctuations) means that a pairwise interaction term cannot be entirely ruled out. It may still be a factor in a more complicated interaction. A secondary conclusion in [15] was that the upper limit on the nearest-neighbour interaction for uncorrelated motion was about 10meV, in good agreement with this. In addition, CO site preferences on the Pt(111) surface, such as those calculated here with DFT, are thought to be of the same order as these interactions. This would tend to counteract the effects of interactions.

When assessing the significance of these results, it is important to take note of the major approximations made in the Monte Carlo simulation. In particular, the lack of different binding sites in the model will rule out any interesting behaviour due to these binding site preferences. As they are on the same scale as the interactions, they may be a significant factor in the dynamics. An important area for further work is to develop a full simulation involving all the sites in each cell. The binding energies for each site calculated from DFT can then be fed into the simulation as parameters. This would then allow accurate calculations at higher coverages, where studies suggest sites other than the top site are particularly important [6-7]. The increased lifetimes for all  $q=0.3$  results do potentially suggest the presence of the  $(\sqrt{3}\times\sqrt{3})R30^\circ$  structure, in agreement with these same studies.

In addition, the effect of including more than just nearest-neighbour interactions should be investigated. Some studies suggest an attractive interaction for separations other than the nearest-neighbours [12], which would almost certainly have an effect on the observed dynamics, generally serving to increase  $\alpha(\Delta k)$  as adatoms cluster together. Other studies suggest a repulsive interaction with for example an inverse-power law dependence on separation [10]. This would probably lead to less correlated motion, as there would no longer be separations that were much more favourable than others.

The DFT calculations carried out here, whilst only preliminary, show a good agreement with previous data. Using this setup, the total energy can be calculated for a range of different separations. Comparing the energy changes for changing separations and structures should suggest a form for any interaction that is present.

## 6. Conclusions

This study attempts to look computationally at pairwise interactions between CO adatoms on a Pt(111) surface. Monte Carlo methods are used to study the decay of the intermediate scattering function over time (by measuring the inverse lifetime) along the  $<11\bar{2}>$  crystal azimuth in  $k$ -space, for varying interaction strengths and coverages. The simulation involves a hexagonal lattice of Pt top sites where CO molecules could bind, with the dynamics determined by a variable strength pairwise interaction. It is shown that for most interaction strengths, including those greater than or equal to most previously proposed values, the change in the inverse lifetime at different  $k$ -points is not uniform for increasing coverage. Rather, some points have much increased lifetimes, corresponding to certain real-space separations having longer lifetimes. This strongly suggests correlated surface diffusion of CO atoms. For each coverage investigated, a cut-off interaction strength is estimated above which motion became correlated. For all but the low coverage measurement, this strength is less than previously proposed interaction strengths. The conclusion of Alexandrowicz *et al.* [15], that helium spin-echo measurements are not consistent with a separable pairwise repulsion, fits well with these results.

## Acknowledgements

Professor David Bird is acknowledged for his attentive supervision and useful advice and tutorials particularly on DFT calculations. In addition, Dr Robert Jack provided useful discussions and pointers on Monte Carlo techniques

## References

- [1] Biloen P and Sachtler W M H 1981 *Adv. Catalysis* **30** 165-216
- [2] Zangwill A 1988 *Physics at Surfaces* (Cambridge: Cambridge University Press)
- [3] Feibelman P J, Hammer B, Norskov J K, Wagner F, Scheffler M, Stumpf R, Watwe R and Dumesic J 2001 *J. Phys. Chem. B* **105** 4018-25
- [4] Yeo Y Y, Vattuone L and King D A 1997 *J. Chem. Phys.* **106** 392-401
- [5] Brown W A, Kose R and King D A 1998 *Chem. Rev.* **98** 797-831

- [6] Ertl G, Neumann M and Streit K M 1977 *Surf. Sci.* **64** 393-410
- [7] Heyden B E and Bradshaw A M 1983 *Surf. Sci.* **125** 787-802
- [8] Kitamura F, Takahashi M and Ito M 1989 *Surf. Sci.* **223** 493-508
- [9] Petrova N V and Yakovkin I N 2002 *Surf. Sci.* **519** 90-100
- [10] McEwen J S, Payne S H, Kreuzer H J, Kinne M, Denecke R and Steinruck H P 2003 *Surf. Sci.* **545** 47-69
- [11] Serra A and Ferrando R 2002 *Surf. Sci.* **515** 588-96
- [12] Zhdanov V P and Kasemo B 2003 *Surf. Sci.* **545** 109-21
- [13] Petrova N V and Yakovkin I N 2005 *Surf. Sci.* **578** 162-73
- [14] Hermse C G M, Jansen M M M, van Bavel A P, Lukkien J J, van Santen R A and Jansen A P J 2010 *Phys. Chem. Chem. Phys.* **12** 461-73
- [15] Alexandrowicz G, Kole P R, Lee E Y M, Hedgeland H, Ferrando R, Jardine A P, Allison W and Ellis J 2008 *J. Am. Chem. Soc.* **130** 6789-94
- [16] Alexandrowicz G and Jardine A P 2007 *J. Phys.-Condes. Matter* **19** 26
- [17] Jardine A P, Hedgeland H, Alexandrowicz G, Allison W and Ellis J 2009 *Prog. Surf. Sci.* **84** 323-79
- [18] Van Hove L 1954 *Phys. Rev.* **95** 249
- [19] Martin R M 2004 *Electronic Structure: Basic Theory and Practical Methods* (New York: Cambridge University Press)
- [20] Dinh V A, Sato K and Katayama-Yoshida H 2010 *J. Supercond. Nov. Magn.* **23** 75-8
- [21] Fukuda A, Takanishi Y, Isozaki T, Ishikawa K and Takezoe H 1994 *J. Mater. Chem.* **4** 997-1016
- [22] Osborne T J and Nielsen M A 2002 *Phys. Rev. A* **66**
- [23] Newman M E J and Barkema G T 1999 *Monte Carlo Methods in Statistical Physics* (New York: Oxford University Press)
- [24] Meng B and Weinberg W H 1994 *J. Chem. Phys.* **100** 5280-9
- [25] Kawasaki K 1966 *Phys. Rev.* **145** 224
- [26] Frigo M and Johnson S G 2009 FFTW Home Page [online]. (Massachusetts Institute of Technology). Available from: <http://www.fftw.org> [15th January 2010].
- [27] Payne M C, Teter M P, Allan D C, Arias T A and Joannopoulos J D 1992 *Reviews of Modern Physics* **64** 1045
- [28] Hohenberg P and Kohn W 1964 *Phys. Rev.* **136** B864
- [29] Kohn W and Sham L J 1965 *Phys. Rev.* **140** A1133
- [30] Gil A, Clotet A, Ricart J M, Kresse G, Garcia-Hernandez M, Rosch N and Sautet P 2003 *Surf. Sci.* **530** 71-86
- [31] Olsen R A, Philipsen P H T and Baerends E J 2003 *J. Chem. Phys.* **119** 4522-8
- [32] PWSCF.org [online]. (DEMOCRITOS National Simulation Center). Available from: <http://www.pwscf.org> [15th January 2010].
- [33] Perdew J P and Zunger A 1981 *Phys. Rev. B* **23** 5048
- [34] Perdew J P, Burke K and Ernzerhof M 1996 *Phys. Rev. Lett.* **77** 3865
- [35] Perdew J P and Wang Y 1992 *Phys. Rev. B* **45** 13244-9
- [36] Orville-Thomas W J 1966 *The Structure of Small Molecules* (Amsterdam: Elsevier Pub. Co.)
- [37] Goldman A S and Krogh-Jespersen K 1996 *J. Am. Chem. Soc.* **118** 12159-66